THE JOURNAL OF PHYSICAL CHEMISTRY B
A JOURNAL OF THE AMERICAN CHEMICAL SOCIETY

pubs.acs.org/JPCB

Article

Nucleation and Growth of Amyloid Fibrils

Sharareh Jalali, Ruoyao Zhang, Mikko P. Haataja, and Cristiano L. Dias*

Cite This: https://doi.org/10.1021/acs.jpcb.3c05300

Read Online

ACCESS | Metrics & More | Article Recommendations | Supporting Information

ABSTRACT: The formation of amyloid fibrils is a complex phenomenon that remains poorly understood at the atomic scale. Herein, we perform extended unbiased all-atom simulations in explicit solvent of a short amphipathic peptide to shed light on the three mechanisms accounting for fibril formation, namely, nucleation via primary and secondary mechanisms, and fibril growth. We find that primary nucleation takes place via the formation of an intermediate state made of two laminated β-sheets oriented perpendicular to each other. The amyloid fibril spine subsequently emerges from the rotation of these β-sheets to account for peptides that are parallel to each other and perpendicular to the main axis of the fibril. Growth of this spine, in turn, takes place via a dock-and-lock mechanism. We find that peptides dock onto the fibril tip either from bulk solution or after diffusing on the fibril surface. The latter docking pathway contributes significantly to populate the fibril tip with peptides. We also find that side chain interactions drive the motion of peptides in the lock phase during growth, enabling them to adopt the structure imposed by the fibril tip with atomic fidelity. Conversely, the docked peptide becomes trapped in a local free energy minimum when docked-conformations are sampled randomly. Our simulations also highlight the role played by nonpolar fibril surface patches in catalyzing and orienting the formation of small cross-β structures. More broadly, our simulations provide important new insights into the pathways and interactions accounting for primary and secondary nucleation as well as the growth of amyloid fibrils.

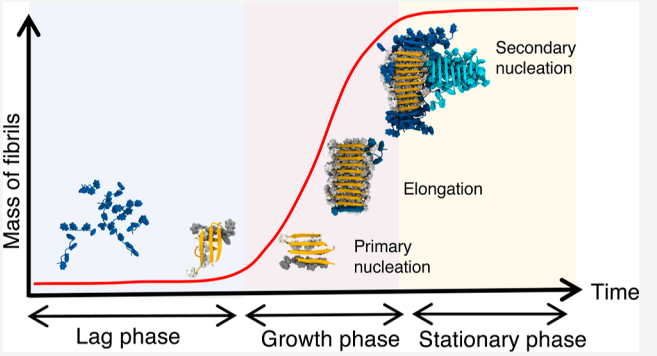

INTRODUCTION

The molecular mechanisms accounting for the aggregation of amyloid peptides into oligomers and fibrils is a topic of intense contemporary research interest.[1−5] This is motivated by the importance of these aggregates in diseases such as Alzheimer's and Parkinson's, as well as by the use of fibrils in various biomedical applications.[6−13] Three processes have been shown to be critical for the formation of amyloid aggregates, namely, nucleation of fibril seeds via primary and secondary mechanisms and the growth of these seeds into micrometer-long fibrils.[14,15] Targeting these processes independently of each other may be required to treat diseases wherein toxic amyloid nuclei need to be inhibited without dissolving already existing fibrils/plaques.[16,17] This level of control requires a detailed molecular-scale understanding of the interactions, pathways, and intermediate structures involved in seed formation and growth, which are poorly understood.

On the one hand, experimental characterization of fibril formation at the molecular level is very challenging due to the dynamic nature and short time scales (macroscopically) involved in seed formation and growth.[3,18] On the other hand, the large number of atoms that must be tracked over extended time scales (microscopically) has made aggregation a difficult process to study computationally.[19−22] Thus, many of the existing theoretical studies of fibril formation have employed either coarse grained models[23−30] or enhanced sampling techniques.[31−37] These studies have provided important insights into the structure of the nucleus of Aβ, which can be made of four or 12 peptides[38,39] and of hIAPP, which may contain significant amounts of α-helices.[40] Additional insights into the pathways accounting for primary nucleation have also been obtained for the short peptides. A case in point is the aggregation of the Aβ_{16-21} peptide, which was shown to emerge in a two-step process at millimolar concentrations where a disordered nucleus forms first, followed by its structural rearrangement into a cross-β structure.[37] In contrast, at submillimolar concentrations, this same peptide was shown to nucleate in one-step without forming disordered aggregates. Using the coarse-grained OPEP force field, the aggregation of the short (KFFE) peptide was shown to proceed bidirectionally, i.e., along the main axis of the β-sheet and via the stacking of different layers of β-sheets on top of each other.[41] Intriguingly, most of the fibril nuclei emerging in

Received: August 4, 2023
Revised: October 19, 2023
Accepted: October 20, 2023

experiments were shown to be catalyzed at the fibril surface (i.e., via *secondary nucleation*)[14,42] with a possible exception reported for the Aβ_{16-22} peptide.[43] Such a catalytic effect of the fibril surface may be related to an increased concentration of peptides in its vicinity and/or to the ability of the surface to align the peptides.

The *growth/elongation* of a fibril, in turn, proceeds via the incorporation of peptides to the fibril tips one peptide at a time.[44−46] It is often described as a *dock-and-lock* mechanism, in which peptides first bind to the fibril ends (i.e., the dock phase) and subsequently sample a range of conformations. The latter process comes to a halt when the incoming peptide aligns itself with fibril end peptides forming parallel or antiparallel β-sheets (i.e., the lock phase).[4,34,47,48] Given that more than $\sim 10^3$ peptides are incorporated into a micrometer-long fibril (each time reproducing the fibril end structure with atomic fidelity), the molecular pathways accounting for the lock phase must be very robust. Two such pathways have been proposed wherein conformational changes take place either randomly, subjected only by steric constraints (i.e., *steric templating* pathway), or driven by side chain interactions between incoming peptides and fibril end peptides (i.e., *direct templating* pathway).[49,50] In addition to the dock-and-lock mechanism, fibril growth can also emerge via a fast-deposition mechanism where peptides adhere to fibril ends in an activated state that enables them to promptly adopt the structure of the fibril without the slow locking phase.[51,52] In all of the aforementioned studies, peptides were assumed to dock directly onto the fibril ends from the bulk solution. However, it is conceivable that peptides deposited on the fibril surface may be able to promptly diffuse to the fibril tip where they can contribute to growth.[53]

In this work, we employ unbiased all-atom simulations in an explicit solvent to provide a more complete microscopic picture of the aggregation process. We show that fibril seeds from amphipathic Ac-(FKFE)$_2$-NH$_2$ peptides emerge spontaneously via primary nucleation, forming a cross-β pattern where the constituent β-sheets are initially oriented perpendicular to each other. This enables the efficient burial of nonpolar residues away from the solvent. However, the growth of these seeds requires the β-sheets to rotate and become aligned with each other, accounting for the formation of the amyloid fibril spine. The growth of an existing fibril in our simulations emerged spontaneously through a dock-and-lock mechanism where peptides landed (or docked) onto the fibril tip from bulk solution or after binding to and diffusing on the fibril surface. At 325 K, electrostatic interactions between charged side chains of the docked peptide and fibril drove the locking process in our simulations, wherein the structure established by the fibril tip is reproduced with atomic fidelity. At 350 K, docked peptides become trapped in local free energy minima while sampling their conformations without ever adopting the structure of the fibril tip. Secondary nucleation is also simulated by adding peptides consecutively to a large simulation box containing a preformed fibril. Finally, the role of nonpolar fibril surface patches in catalyzing the transformation of small aggregates into cross-β structures is highlighted in these simulations.

METHODS

Peptide Chemistry. In this paper, we study the self-assembly mechanisms of an amphipathic peptide made from eight residues that alternate between nonpolar and charged amino acids. Phenylalanine, represented by the one amino acid letter code **F**, is used as the nonpolar amino acid. Positive lysine (**K**) and negative glutamic acid (**E**) are used for charged amino acids. The peptide is capped with acetyl (Ac) and amide (NH_2) groups at N- and C-terminal, respectively, accounting for the neutral Ac-(**FKFE**)$_2$-NH$_2$ sequence—see Figure 1a.

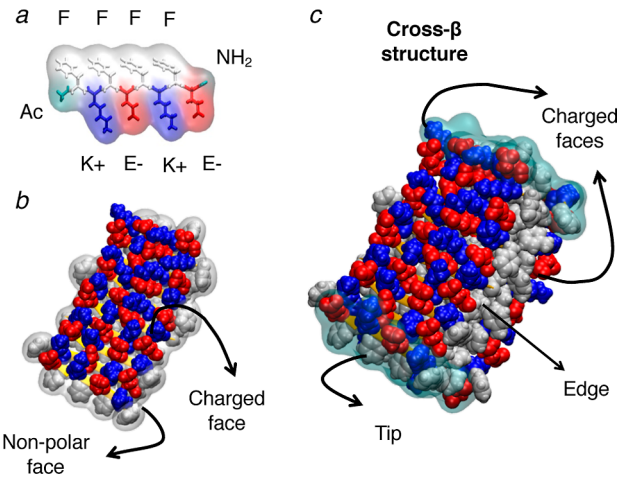

Figure 1. Amino acid sequence, β-sheet, and amyloid fibril from an amphipathic peptide. (a) Nonpolar phenylalanine (F), positively charged lysine (K), and negatively charged glutamic acid (E) are the three amino acids used to account for the amphipathic Ac-(FKFE)$_2$-NH$_2$ peptide. (b) Nonpolar and charged residues are segregated to different faces of antiparallel β-sheet. (c) Packing of nonpolar faces of two β-sheets against each other accounts for the cross-β structure of amyloid fibrils. Nonpolar edges and tips are highlighted in the figure.

This peptide was shown to promptly self-assemble into amyloid-like fibrils both experimentally and in computer simulations.[54−58] Furthermore, recent cryo-EM images revealed that the supramolecular assembly of these fibrils emerges from the concentric juxtaposition of four- and six-fibrils accounting for *thin* and *thick* nanotubes.[59]

Force Field and System Equilibration. Molecular dynamics simulations were performed with the Amber99sb-ILDN force field[60] and the TIP3P water model using cubic boxes and periodic boundary conditions in the isothermal−isobaric (*NPT*) ensemble. The Parrinello−Rahman barostat (τ_p = 2.0 ps) was employed to maintain the pressure of the system at 1 bar.[61] Temperature was controlled by coupling protein and solvent separately to a velocity-rescaling thermostat (τ_t = 0.1 ps). The equations of motion were integrated using the leapfrog algorithm with a 2 fs time-step.[62] The cutoff for short-range van der Waals and electrostatic interactions was 1.0 nm, and the smooth Particle Mesh Ewald algorithm was used to compute long-range electrostatic interactions.[63] All of the systems studied here were equilibrated in the *NVT* and *NPT* ensembles for 100 ps. All simulations were conducted using the 2020 version of GROMACS.[64] Descriptions of the different setups used to study primary and secondary nucleation as well as fibril elongation are provided in the Results and Discussion Section.

Analysis. Various quantities were used to analyze the different trajectories using the GROMACS toolkit. This includes the minimal distance between the backbone atoms of two peptides and the peptide secondary structure content computed using DSSP. GROMACS was also used to compute a list containing all pairs of peptides that are at a distance of

https://doi.org/10.1021/acs.jpcb.3c05300
J. Phys. Chem. B XXXX, XXX, XXX−XXX

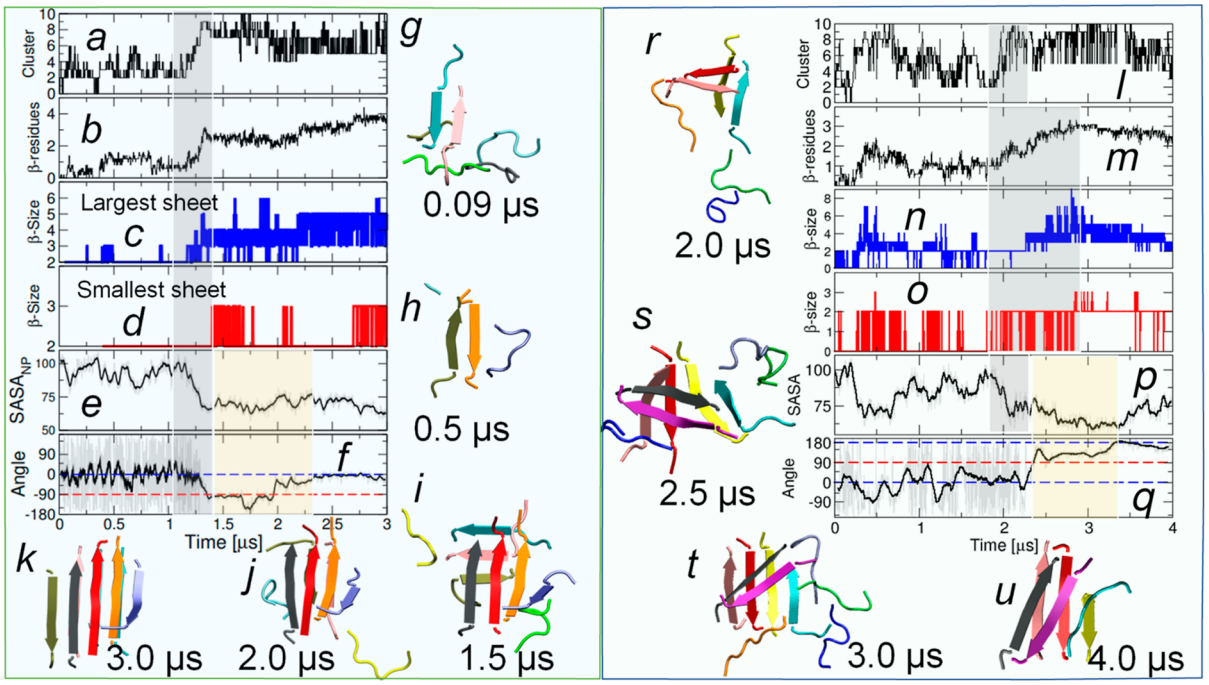

Figure 2. Observation of primary nucleation in two independent simulated trajectories. The time dependences of various quantities are computed to characterize the spontaneous formation of cross-β structures. These quantities are (a,l) the largest cluster size in the simulation box, (b,m) the number of residues per peptide in a β-structure, the number of peptides comprising (c,n) largest and (d,o) second largest β-sheet in the simulation box, (e,p) SASA of nonpolar residues, and (f,q) dihedral angle between peptides of largest and second largest β-sheets. The formation of a stable oligomer and the existence of a perpendicular cross-β structure are highlighted by gray and orange rectangles. Conformations of the largest cluster at select times are shown in panels (g–k and r–u) for the two independent trajectories. A different color is used for each peptide for visualization purposes.

less than 0.5 nm from each other. This list is used as input for an in-house code to compute the size of the largest aggregate (or cluster) made from peptides that are in contact with each other. A description of the algorithm behind the code is given on pages S10–S11. The number of peptides within the largest cluster is used to determine the formation of stable nuclei during primary nucleation. It is also used to compute the growth of a seed during secondary nucleation.

The geometry of the hydrogen (H), donor (D), and acceptor (A) atoms is used to define the formation of hydrogen bonds. In particular, a hydrogen bond is formed if the donor–acceptor distance is less than or equal to 0.35 nm and the H–D–A angle is found to be less than 30°. Using this default definition, peptides are considered to be part of a β-sheet if they form at least four backbone hydrogen bonds with each other. This was used to determine the number of peptides forming each of the two β-sheets in the cross-β structure in primary nucleation.

Simulation Setup. *Primary Nucleation.* To provide insights into the formation of a fibril nucleus in bulk solution, extensive simulations were performed with 10, 15, and 20 peptides embedded randomly in large solvated boxes of dimension 13 × 13 × 13 nm^3 corresponding to 7.5, 11.3, and 15.1 mM peptide concentrations, respectively. This investigation started with one independent simulation at each of these three concentrations performed for 1.5 μs. A stable cluster containing most of the peptides formed before the end of the trajectory in all of these simulations. These clusters exhibit the cross-β pattern that is characteristic of amyloid fibrils wherein nonpolar residues of two β-sheets are buried against each other. In simulations performed at the highest concentrations (i.e., 15.1 and 11.3 mM), these clusters emerged promptly within 0.25–0.5 μs, making it difficult to identify the sequence of events leading to their formation—see Figures S1 and S2. Therefore, the main results of our study on primary nucleation were obtained at 7.5 mM. To provide meaningful results, two systems in total were simulated at this concentration for up to 4 μs.

Fibril Growth. To investigate the mechanisms accounting for fibril growth, all-atom simulations were performed in a solvated box of size 10.1 × 10.1 × 10.1 nm^3 containing a preformed fibril and a peptide. The fibril is constructed by packing nonpolar faces of two antiparallel β-sheets made from 10 Ac-(FKFE)$_2$-NH$_2$ peptides against each other—see Figure 1. This corresponds to class 5 of the amyloid spine classification scheme by Eisenberg and Sawaya.[65] The simulation box is prepared in a three-step process. First, the preformed fibril is inserted into the box using the *insert-molecules* command of GROMACS. Second, the free peptide is added to the box using the same command. Third, if the computed minimal distance between the peptide and the fibril is smaller than 2 nm, the peptide is removed from the box, and a new insertion is attempted. The third step is repeated until the peptide is at a distance larger than 2 nm from the fibril. After this requirement is met, the box is solvated with TIP3P water molecules, and simulations are performed at 298, 325, and 350 K.

Secondary Nucleation. To investigate the secondary nucleation mechanism, we have therefore performed six simulations with six peptides in 13 × 13 × 13 nm^3 boxes containing one preformed fibril at 350 K. First, the preformed fibril is inserted into the box, and second, the free peptides are

https://doi.org/10.1021/acs.jpcb.3c05300
J. Phys. Chem. B XXXX, XXX, XXX–XXX

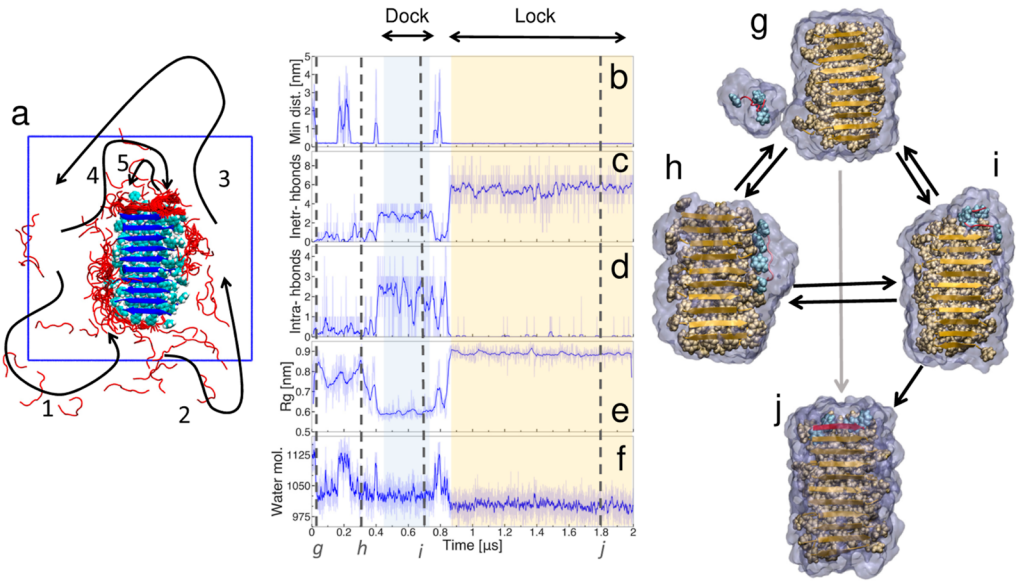

Figure 3. Unbiased pathways accounting for fibril elongation. (a) Trajectory of the peptide as it interacts with the fibril before docking to its tip is shown. The conformations of the peptide (red) are depicted every 20 ns. Numbered arrows show the progression of the peptide in the simulation. The fibril is depicted using a cartoon representation in blue and a van der Waals representation for phenylalanine side chains in cyan. The time dependence of five quantities are computed to characterize the peptide−fibril complex: (b) minimum distance between atoms of the fibril and the peptide, (c) inter- and (d) intrabackbone hydrogen bonds, (e) radius of gyration of the peptide, and (f) number of water molecules around peptide and fibril. Sample configurations of the peptide−fibril complex when the peptide is (g) fully solvated, (h) bound to the fibril surface, (i) docked, and (j) locked onto the fibril tip. Arrows highlight possible transitions between the different states.

placed randomly in the simulation box using gmx insert-molecules.

RESULTS AND DISCUSSION

Primary nucleation. *Nucleus Formation.* Figure 2a,b and l,m depicts the size of the largest cluster and the number of residues making up β-sheet structures in two independent simulations performed at 7.5 mM. Clusters form and dissociate within the first 1 and 2 μs of the first and second trajectories, respectively. These intermittent clusters are mostly dimers and trimers in the first trajectory (see panels g,h) but also heptamers and tetramers in the second trajectory.

In the first simulation, a stable nucleus comprising 6−8 peptides emerges at 1.25 μs, as can be seen in the cluster size data (panel a) and the number of β-residues (panel b), see the gray shade. These data characterize a one-step nucleation process in which the nucleus is formed in an orderly manner.[66] In the second simulation, a stable nucleus comprising 6−8 peptides forms after 2.0 μs. In the latter process, the cluster size increases within a short time-window of 0.2 μs (see panel l), while the number of β-residues (see panel m) increases slowly over ∼1 μ s—see gray shades. These data, in turn, characterize a two-step nucleation process, wherein aggregation takes place with a significant amount of disorder, requiring subsequent conformational changes to complete the process. The existence of different time scales for aggregation and conformational ordering of peptides is also observed in our high-concentration simulations (i.e., 11.3 and 15.1 mM). In the latter, the number of β-residues increases long after the cluster size has saturated. The relaxation times associated with this conformational change can be obtained by computing the autocorrelation function of β-residues. However, for this quantity to be meaningful, more than one replica at 11.3 and 15.1 mM needs to be simulated, which is beyond the scope of the current study. These results are consistent with a recent study showing that the Aβ_{16-21} peptide undergoes a one-step nucleation process at low concentrations and a two-step process at high concentrations.[37]

Perpendicular and Parallel Cross-β Structures. To characterize the structure of the nucleus, panels c−d and n−o depict the size of the two largest β-sheets in the system in the one- and two-step nucleation processes. Also, panel e,p depicts the solvent accessible surface area of nonpolar residues, i.e., SASA. These panels show that the two β-sheets increase in size during/after the formation of a nucleus (i.e., the gray shaded area), and this coincides with a significant decrease in SASA as nonpolar residues of the two β-sheets become buried away from the solvent. This characterizes the cross-β pattern of amyloid fibrils for which a representative structure is depicted in panel i. In the two-step nucleation process, the early aggregate, which formed at ∼2 μ s, also exhibits two β-sheets with nonpolar residues buried against each other and with disordered peptides around them; see panel r. These disordered peptides become incorporated into the two β-sheets within time 2 and 3 μs (see panels s−t).

Clusters formed via one-step [panel (i) and two-step (panel r−t)] processes exhibit two β-sheets that are initially oriented perpendicular to each other. They remain in that configuration for more than 0.5 μs before reorienting themselves to become aligned with each other (see panels j, k, u, and Movie S1). This process is quantified in panels f and q (orange shades in panels f,q), which show the time dependence of the dihedral angle between peptides on opposing β-sheets. Initially, in the trajectory, the dihedral angle can take any value from −180 to 180° as peptides move freely in the simulation box; see the light gray line. As the early nucleus is formed, the dihedral angle adopts values close to −90 or 90°, which is indicative of perpendicular cross-β structures. In panel f, this takes place between 1.25 and 2 μs. Subsequently, the dihedral angle changes to ∼0° as the β-sheets become parallel to each other.

https://doi.org/10.1021/acs.jpcb.3c05300
J. Phys. Chem. B XXXX, XXX, XXX−XXX

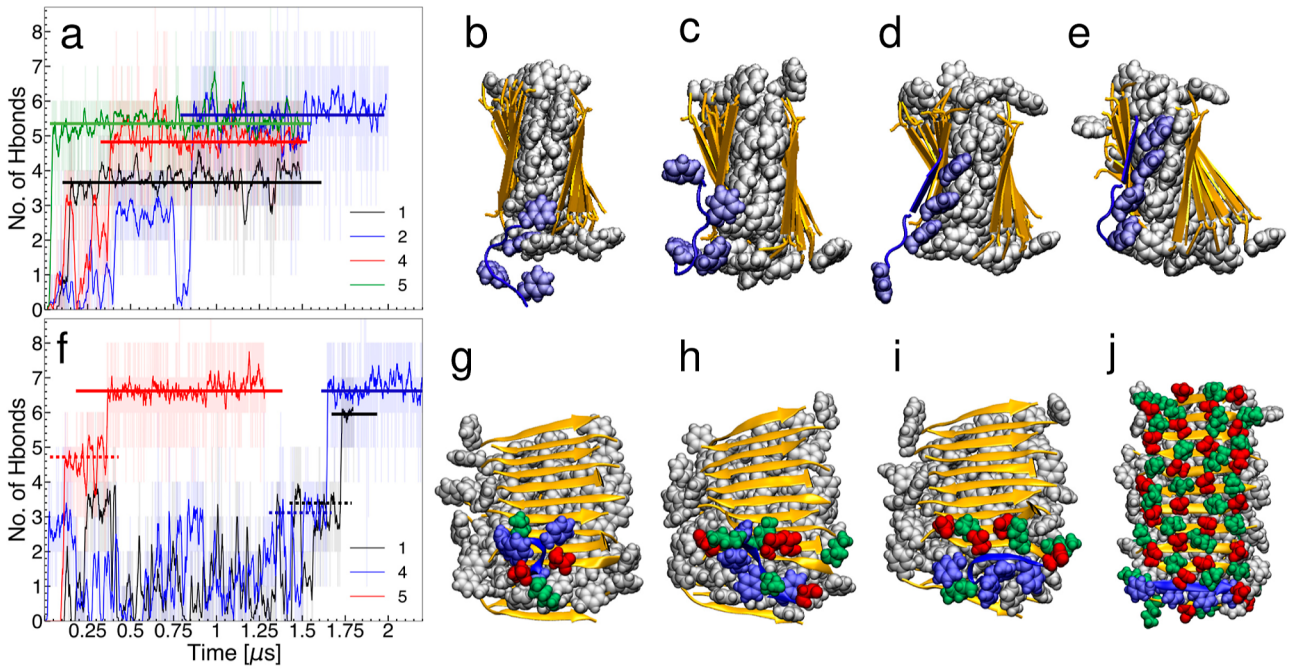

Figure 4. Locking of the peptide to the fibril tip. The time dependence of the number of interbackbone hydrogen bonds between peptide and fibril at (a) 350 and (f) 325 K. The structure of the peptide−fibril system in trajectory number 4 at 350 K is represented at time (b) 0.16, (c) 0.37, (d) 0.57, and (e) 0.90 μs. The structure of the peptide−fibril system of trajectory number 5 at 325 K is shown at time (g) 0.09, (h) 0.11, (i) 0.2, and (j) 1.01 μs. A van der Waals representation is used for nonpolar residues of the fibril (white) and peptide (blue). Negatively charged glutamic acid and positively charged lysine are colored red and green, respectively.

Similarly, for panel q, the dihedral angle adopts values close to 90° between time 2.5 and 3.25 μs. This is followed by an increase in the dihedral to 180° characterizing parallel β-sheets—see panel u.

Note that the average SASA (panel e) of perpendicular and parallel nuclei are very similar in magnitude despite β-sheets being made of more peptides in the latter. This suggests that nonpolar residues can bury themselves more efficiently in perpendicular cross-β structures, which could be the force driving the formation of these structures. However, perpendicular cross-β structures need to rotate for the early nucleus to grow, as peptides cannot be incorporated indefinitely into β-sheets that are perpendicular to each other while shielding their nonpolar residues from water.

Fibril Growth. *Addition of Peptides to Fibrils.* Figure 3a depicts the trajectory of a free-peptide as it binds to and unbinds from a preformed fibril in one of our simulations at 350 K. Backbone conformations of the free-peptide (in red) are shown at every 20 ns, while numbered arrows indicate the sequence of events in the simulation. The peptide explores several nonpolar binding sites at the edges and tips of the fibril, but it rarely binds to the charged faces of the fibril. To quantify these binding and unbinding events, panel b shows the time dependence of the minimum distance ξ between atoms of the peptide and the fibril. The peptide, which is initially in the solution (i.e., $\xi > 2$ nm), is attracted to the fibril in less than 0.025 μs where it binds ($\xi \leq 0.2$ nm) and remains bound for approximately 0.125 μs. The peptide then detaches to become fully solvated. It undergoes three other such binding-unbinding events until time ∼0.8 μs when it locks onto the fibril tip. It remains locked until the end of the simulation, i.e., for more than 1.2 μs.

To further characterize the state of the system, panels c,d depict the numbers of inter- and intrabackbone hydrogen bonds of the peptide. When it is solvated (i.e., ξ is larger than 0.2 nm) or bonded to the sides/edges of the fibril, the number of interpeptide hydrogen bonds is essentially negligible. This quantity is non-negligible only when the peptide binds to the fibril tip, as highlighted by the blue and yellow shades. The number of intrapeptide hydrogen bonds, in turn, is non-negligible only when the peptide adopts a folded conformation. In the blue shaded region in Figure 3, the peptide adopts a "hairpin"-like conformation, while docked onto the fibril tip. This binding event lasts for approximately 0.3 μs, after which the peptide detaches from the fibril tip while retaining its hairpin-like conformation. The radius of gyration, which quantifies the compactness of the peptide, is shown in panel e. This quantity is maximum when the peptide is locked into the fibril tip (see yellow shade), and it is minimum when the peptide is folded into a hairpin-like conformation—see the region shaded in blue. Finally, while fully solvated or on the fibril surface, the radius of gyration adopts intermediate values.

Panel f shows the number N_{shell} of water molecules within a distance of 0.4 nm from either the peptide or the fibril. The number of shell-water molecules is a maximum when the free-peptide is fully solvated. As it interacts with the fibril, desolvation takes place as some shell-water molecules are released into the bulk, accounting for a reduction in N_{shell}. The number of shell-water molecules in panel f is minimal when the free-peptide locks onto the fibril tip—see the region shaded in yellow. Note that when the fibril grows by one layer, the structure of the fibril end is reproduced with atomic fidelity, and the number of shell water molecules around the end does not change significantly. Thus, the reduction in N_{shell} when the peptide locks onto the fibril end must be due to shell-water molecules around the free-peptide released into the bulk. The release of shell-water molecules into the bulk is a highly favorable entropic process around nonpolar residues,[67−71]

https://doi.org/10.1021/acs.jpcb.3c05300
J. Phys. Chem. B XXXX, XXX, XXX−XXX

contributing to the thermodynamic driving forces for elongation.[31−34]

Transitions between Different Peptide−Fibril Binding Modes. The quantities depicted in Figure 3b−f highlight the different states of the peptide in which it can be fully solvated, bound to the fibril edge, as well as docked and locked to the fibril tip (see panels g−j). Six additional simulations (i.e., seven in total) were performed at 350 K to provide insights into the transitions between these different states. In all seven simulations, the peptide locked onto the fibril tip where it remained until the end of the simulation, i.e., for longer than 0.5 μs. In two and five of these simulations, the peptide formed antiparallel and parallel β-sheets with the fibril, respectively. Moreover, the quantities shown in Figure 3b−f were computed for all simulations, and the state of the peptide was determined at all times—see Figure S3b.

In three of the seven simulations, the peptide became incorporated into the fibril tip in less than 0.15 μs. In these simulations, the peptide diffused in the bulk solution before being docked onto the tip. This was followed by the peptide promptly (in less than 0.01 μs) changing its conformation to lock onto the fibril tip. This characterizes a "fast-deposition" process in which the peptide is deposited at the tip in an activated state that requires only a few conformational changes to reproduce the template imposed by the fibril tip.[51,52] This process is symbolized in Figure 3g−j by the gray arrow. In the other four simulations, the peptide is also found to lock itself onto the fibril tip within less than 2 μs. This occurred after the peptide reached the tip either from the solution or after diffusing along the fibril surface. Out of the 7 simulations performed at 350 K, in 4 and 3 of them, the peptide landed on the tip after diffusion in the solution and along the surface of the fibril, respectively. At the tip, the docked peptide can detach itself to become solvated, diffuse back to the fibril edge, or lock itself onto the fibril tip. These observed transitions in our simulations highlight the diversity of pathways, shown by arrows in Figure 3g−j, by which a peptide can lock itself onto the fibril tip. Estimates of the transition rates between these states and how they can be used to develop continuum models of fibril growth are provided elsewhere.[72]

Effects of Temperature. To provide insights into the effects of temperature on the dock-and-lock mechanism, five simulations were also performed at both 298 and 325 K—see Figure S4a,b. In three of the five simulations at 325 K, the peptide ended up locked in an antiparallel β-sheet conformation, forming ∼7 interbackbone hydrogen bonds with the tip. In two of these simulations, the peptide reached the tip by diffusing along the fibril edge. At 298 K, some of the five simulations were extended up to 4 μs, and in only one of them did the peptide lock onto the fibril tip. Thus, at a lower temperature (both 325 and 298 K), most of the simulation time is spent with the peptide on the fibril surface, and consequently, much longer simulations are required to observe locking. This implies that the fibril surface plays an important role in the kinetics of growth by adsorbing peptides onto it.

Locking onto the Fibril Tip. Figure 4 illustrates the process by which the peptide samples different conformations prior to locking onto the fibril tip at 350 K (upper panels) and at 325 K (lower panels). Panel a shows the number of hydrogen bonds between peptide−fibril backbone atoms (N_{HB}) in four trajectories at 350 K. In most trajectories, N_{HB} increases abruptly after the peptide lands on the fibril tip. In this process, at least one of its phenylalanine side chains remains in contact with the fibril tip at all times, while the other nonpolar side chains are free to move and probe different interaction sites at the tip—see panels b−e. These processes are facilitated by the elevated temperature employed in the simulations and associated thermal fluctuations. The latter is overcome when a sufficient number of bonds are formed between the peptide and the fibril without necessarily accounting for the proper alignment. Accordingly, in two trajectories, the peptide formed parallel (instead of antiparallel) β-sheets at the tip. Moreover, within the time frame of the simulation (i.e., at least 1.5 μs), N_{HB} does not change significantly after 4−6 hydrogen bonds have formed (see panel a), whereas a perfect alignment of the peptide with the fibril requires the formation of at least seven hydrogen bonds. Accordingly, the atomic structure of the tip is never reproduced by the peptide in any of the seven simulations performed at 350 K—see Movie S2.

Panel *f* depicts N_{HB} for the three simulations in which the peptide locks onto the fibril tip at 325 K. At this temperature; the locking process takes place in two-steps highlighted by dashed and full lines. An increase in N_{HB} from zero to 3−5 (dashed lines) accounts for the first step, which lasts for 0.1−0.3 μs. The second step emerges from another increase in N_{HB} to approximately seven hydrogen bonds. The latter gives rise to configurations in which the peptide is aligned with the fibril, forming antiparallel β-sheets in all three simulations. To show how the peptide becomes aligned with the fibril, characteristic configurations during the lock phase are shown in panels g−j for trajectory number 5, i.e., the red line in Figure 4f. Panel g shows that the peptide lands on the tip in a random conformation with some of its nonpolar side chains buried away from the solvent. Conformations highlighting the first step of the lock phase are depicted in panels h,i. They are characterized by the alignment of the C-terminal of the peptide with the fibril, wherein charged side chains of the peptide interact with oppositely charged side chains of the fibril. The peptide remains in this configuration for more than 0.2 μs until charged side chains at the N-terminal of the peptide become aligned with charged side chains of the fibril—see panel j and Movie S3. This type of stepwise alignment of the peptide contrasts with the random sampling observed at higher temperatures.

Our simulations give rise to results that at first sight appear counterintuitive: peptides docked onto the fibril tip are more likely to find the global minimum at a low temperature than at a high temperature where they become trapped in local minima. This emerges because electrostatic interactions between charged side chains are disrupted by thermal fluctuations at high temperatures and cannot drive the alignment of the peptide. Thus, a random conformational search takes place until a significant number of peptide−fibril bonds is formed, trapping the peptide at the tip without necessarily accounting for the proper alignment. At low temperatures, the peptide becomes aligned with the fibril in a stepwise manner wherein charged side chains at one extremity of the peptide are aligned first, followed by the other extremity. The latter process enables the structure of the fibril to be reproduced with atomic fidelity.

Secondary Nucleation. Secondary nucleation begins with the attraction of peptides to the fibril surface, enabling the local peptide concentration to reach a critical value required to form a stable nucleus. The adsorption of peptides onto the fibril edge in our simulations (see Figure 3) hints at the possibility of secondary nucleation being a mechanism of fibril formation for

https://doi.org/10.1021/acs.jpcb.3c05300
J. Phys. Chem. B XXXX, XXX, XXX−XXX

the Ac-$(FKFE)_2$-NH_2 peptide. However, the formation of a nucleus requires more than one peptide to be present in the simulation box.

Seed Formation and Growth. Figure 5 shows the final conformations of six 2 μs long simulations in which six peptides are initially located randomly in the simulation box with a pre-formed fibril Figure 5. In four of these simulations (panels a−d), most of the six peptides contributed to the elongation of the fibril by locking onto its tip. In two of the simulations (panels e,f), the majority of the peptides formed oligomeric structures at the fibril edge. In particular, a single β-sheet and a cross-β structure became adsorbed onto the fibril edge in panels e and f, respectively. In these two simulations, the sequence of events leading to the formation of oligomeric structures is illustrated in Figure 6. In both cases shown in panels a and b, two or three peptides are attracted toward each other at the edge of the fibril where they form small aggregates. Nonpolar residues of these aggregates reduce their exposure to the solvent by facing the edge of the fibril and/or by facing nonpolar residues of nearby peptides. This leads to the formation of a small β-sheet made from two peptides at time 0.54 μs in panel a, which elongates into a pentamer at the end of the simulation. In panel b, a small cross-β structure formed early in the simulation (i.e., at 0.37 μs) and remained stable until the end of the simulation.

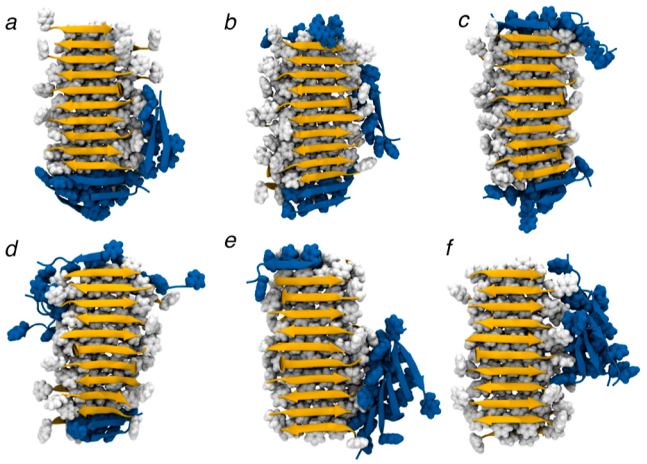

Figure 5. Final conformations of 2 μs long simulations in which six peptides initially randomly located in the simulation box are allowed to interact with a preformed fibril. A van der Waals representation is used for nonpolar residues of the fibril (white) and peptide (blue). A cartoon representation is used for the backbone of the fibril (orange) and peptide (blue).

To study the growth of stable seeds on the fibril surface, we added six additional free peptides to the solvated box containing the configuration shown in Figure 5f. These free peptides are at an initial distance of at least 2 nm from the fibril-seed complex. A 0.5 μs long simulation of this system was carried out at 350 K, and its final configuration was used as the starting point of a new simulation with six peptides added to the box. This process of adding six solvated peptides to the simulation box was repeated another three times such that the final box comprised 36 added peptides and a preformed fibril made of 20 peptides. Final configurations after each of these steps are depicted in Figure 7 showing the growth of both the preformed fibril and the seed. Figure 8 shows the numbers of peptides incorporated onto fibril tips and seed as a function of time. Despite large fluctuations, the number of peptides incorporated into the seed is equal to or larger than the number accounting for fibril growth except during the last 0.5 μs of simulations. This is surprising as one would expect a growth rate twice as large for the preformed fibril that has two tips exposed to the solvent at any given time. One may speculate that the larger exposure of nonpolar side chains around the seed's tip enables it to adsorb peptides more readily than either of the fibril tips. Interestingly, the nonpolar edge of the preformed fibril located on the opposite side of the nucleus is mostly depleted of added peptides at the end of the simulation—see Figure 7e. This accumulation of peptides on just one of the nonpolar faces of fibrils was also observed in discrete molecular dynamics simulations.[30]

Recent cryo-EM studies have shown that Ac-$(FKFE)_2$-NH_2 peptides form nanotubes comprising four or six amyloid fibrils with the main axis pointing in the same direction while concentrically distributed around the surface of a cylinder. The formation of these supramolecular structures may start with the nucleation of distinct fibrils in solution, which subsequently come together to form nanotubes. While such a scenario for nanotube formation is plausible, primary nucleation takes place at a much slower rate than secondary nucleation for most amyloid peptides. Thus, a more compelling scenario is that of one fibril forming via primary nucleation and the other fibrils accounting for the nanotube catalyzed at its surface. Our simulations show that such catalyzed fibrils emerge perpendicularly (not parallel) to the parent fibril. Accordingly, parent and daughter fibrils have to rotate in order to become aligned with each other, which could be driven by hydrophobic interactions between nonpolar edges of emergent and parent fibrils. Thus, nanotube formation may emerge from nucleation events at the surface of parent and daughter fibrils followed by rotation. While this proposed mechanism of nanotube formation is admittedly speculative, its initial steps, including the orientations of daughter fibrils with respect to parent fibrils, are supported by our simulations.

CONCLUSIONS

In summary, the unbiased nature of our simulations allowed us to provide new insights into the pathways accounting for the nucleation and growth of amyloid fibrils from a short amphipathic peptide. In particular, we identified a new intermediate state (i.e., the perpendicular cross-β pattern) on the pathway to primary nucleation—see Figure 9. We also report on a new docking mechanism by which peptides reach the fibril tip by diffusing along its surface; see Figure 9. Our simulations suggest that this pathway contributes significantly to populate the fibril tip with peptides. Our simulations are also contributing to the debate of how peptides lock onto the fibril tip. In particular, we found that peptides are not able to align themselves with the template provided by the fibril tip by randomly sampling over different conformations. This alignment was, however, reproduced with atomic fidelity when the conformational change of the docked peptide was driven by side chain interactions between charged residues; see Figure 9. Thus, we anticipate that screening the electrostatic interactions by adding salt to the solution may have a strong effect on the locking process of our amphipathic peptide. Our simulations also provided new insights into the aggregation of peptides on the fibril surface (Figure 9).

The novel insights brought up by this study required tracking a large number of atoms (more than 200,000 atoms to

https://doi.org/10.1021/acs.jpcb.3c05300
J. Phys. Chem. B XXXX, XXX, XXX−XXX

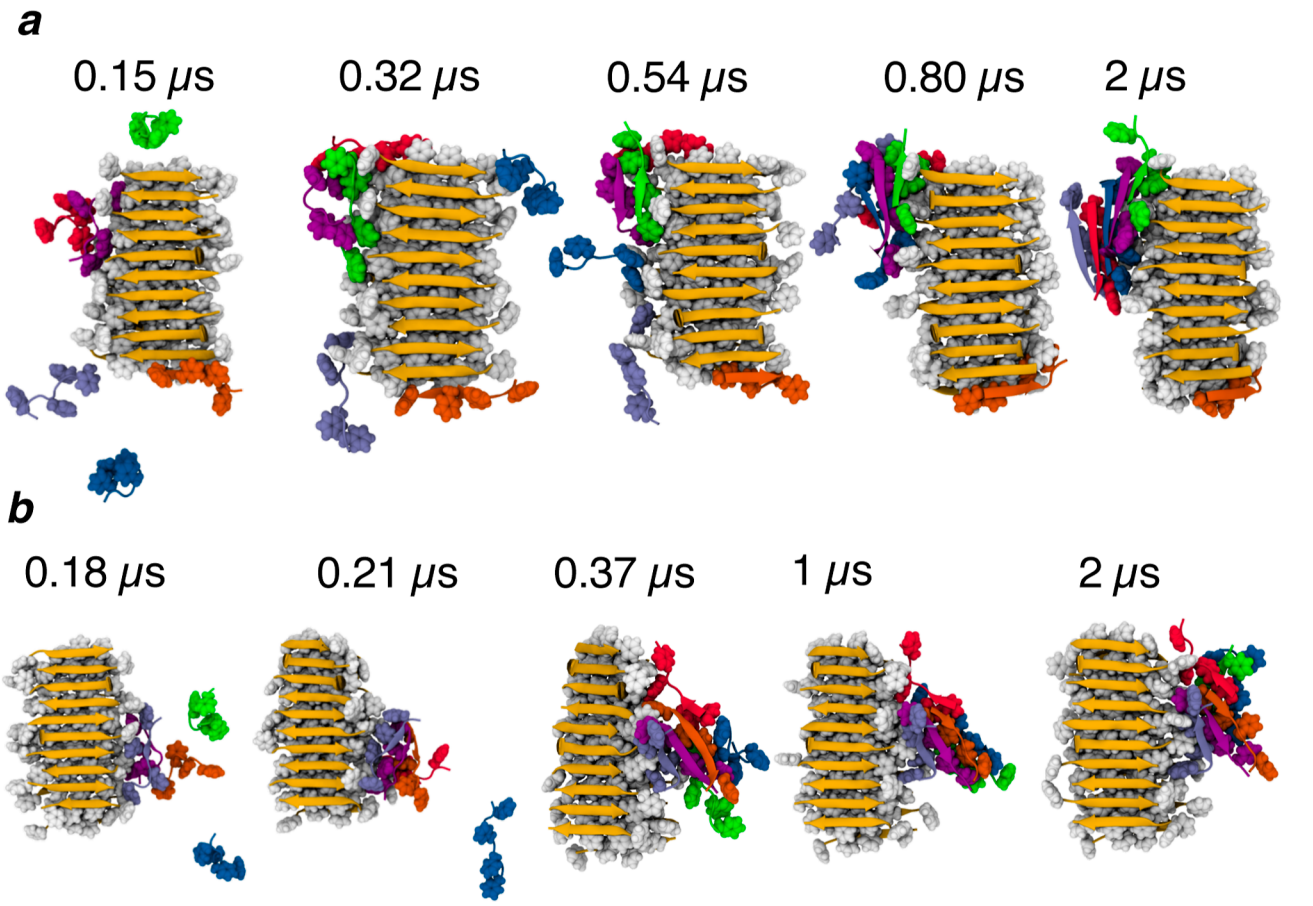

Figure 6. Sequence of events leading to the formation of a nucleus on the surface of a preformed fibril (in orange and white) from six peptides deposited randomly in the simulation box. (a) Events leading to the formation of the structures in Figure 5e. (b) Events leading to the structure in Figure 5f. Each peptide is shown by using a different color.

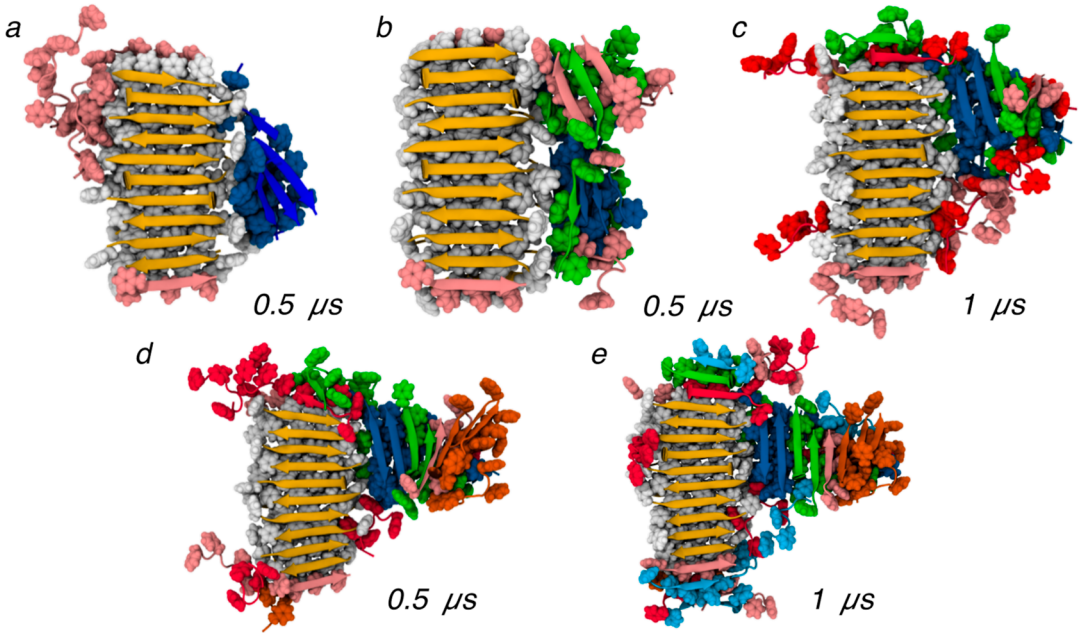

Figure 7. Growth of a new nucleus (blue) on the surface of a preformed fibril (white and yellow) through the consecutive addition of six peptides to the simulation box. Peptides are colored pink, green, red, orange, and cyan according to the order in which they are added to the simulation box. After each addition of six peptides, a 0.5 or a 1 μs simulation (as indicated in the figure) is performed to allow peptides to bind to the fibril. Final configurations are shown with the backbone of the preformed fibril illustrated in orange using a cartoon representation. A van der Waals representation is used for nonpolar residues.

https://doi.org/10.1021/acs.jpcb.3c05300
J. Phys. Chem. B XXXX, XXX, XXX−XXX

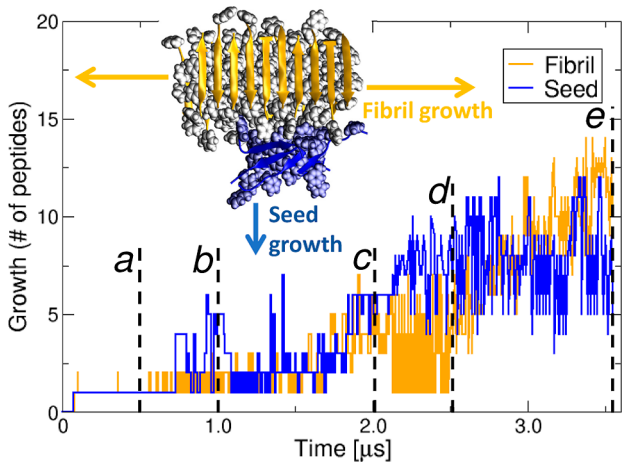

Figure 8. Growth of the parent fibril and seed. Orange and blue lines correspond to the number of peptides incorporated into the fibril and seed, respectively. Dashed horizontal lines indicate the instant when six new peptides are introduced to the solution. Labels (a−e) refer to the configurations in Figure 7.

account for peptide concentrations of ∼10 mM) over extended time scales (>2 μ s).[18,19,54] The extensive computational resources required for such calculations were previously not easily accessible to the scientific community. Accordingly, previous unbiased all-atom simulations in an explicit solvent were mostly performed in boxes containing a small number (<10) of short peptides and on time scales that were too short to allow for both the formation of cross-β structures and docking via surface diffusion. Therefore, these studies provided only rather limited insights into the existence of intermediate states and overlooked the surface-docking pathway. In the same vein, the time scale associated with locking onto the fibril tip is beyond the reach of all-atom simulations for full-length amyloid peptides. Thus, previous computational studies have focused on the dissociation of peptides from the tip, and insights into the locking phase were obtained using coarse-grained models.[4,25]

It is important to highlight that simulations in this study were performed at elevated temperatures (325 or 350 K) to accelerate the aggregation process.[20] This allowed us to investigate fibril formation in a reasonable time frame. As computers are becoming faster, we anticipate that it will soon be possible to test the mechanisms put forward by our simulations at ambient and body temperatures. Moreover, additional simulations will be helpful to further validate the proposed mechanisms observed in the present work using a rather limited number of replicas due to the computational cost of these simulations. In the same vein, it may soon be possible to study larger systems containing fibrils and small aggregates dispersed in solution in order to understand how they compete for monomers. It will also be relevant to test the scope of our results for other peptide sequences. Are perpendicular cross-β structures intermediate states for a broad class of peptides? Do all peptides populate the fibril tip via a combination of bulk- and surface-docking pathways? If full-length amyloid peptides fall within the same class of peptides as $(FKFE)_2$, the microscopic mechanisms proposed here will have important implications for reducing amyloid toxicity in diseases.

With regard to the surface-docking pathway, we have recently developed an integrated approach combining MD simulations with continuum theory to address this intriguing question.[72] Specifically, our work shows that surface-docking indeed is expected to contribute to fibril growth kinetics for

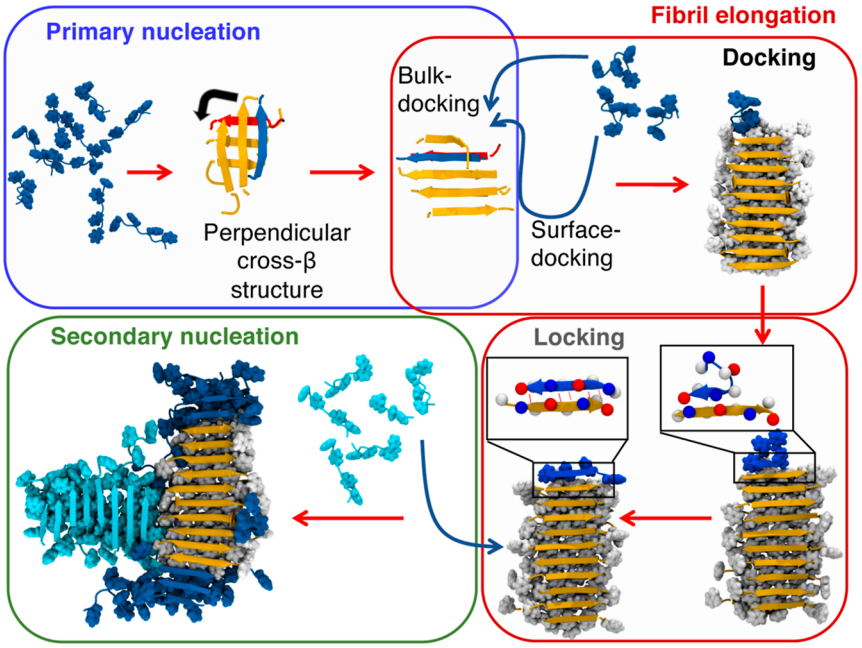

Figure 9. Schematic representation of the intermediate states and pathways accounting for fibril formation of Ac-$(FKFE)_2$-NH_2 peptides in our simulations. BLUE: primary nucleation proceeds via the formation of perpendicular cross-β structures. Rotation of the β-sheets in the latter leads to the emergence of the amyloid spine. RED (Upper): docking proceeds with peptides diffusing in solution or on the fibril edge to land on the tip. RED (Bottom): stepwise-locking proceeds with the alignment of side chains at different extremities of the peptide with the fibril. Positively charged residues (K) and negatively charged residues (E) are shown in blue and red, respectively. GREEN: peptides (light blue) aggregate at the nonpolar edge of the fibril where new fibrils are nucleated.

https://doi.org/10.1021/acs.jpcb.3c05300
J. Phys. Chem. B XXXX, XXX, XXX−XXX

generic peptide sequences, with the efficacy of the pathway controlled by peptide diffusivities in the bulk solution and on the fibril surface as well as peptide binding/unbinding rates to/from the fibril surface.

■ ASSOCIATED CONTENT

Supporting Information

The Supporting Information is available free of charge at https://pubs.acs.org/doi/10.1021/acs.jpcb.3c05300.

Results of simulations performed to study primary nucleation at concentrations of 11.3 and 15.1 mM, description of simulations performed to study fibril growth with raw data, description of simulations performed to study secondary nucleation, description of movies used to illustrate primary nucleation, and locking at 350 and 325 K (PDF)

■ AUTHOR INFORMATION

Corresponding Author

Cristiano L. Dias − *Department of Physics, New Jersey Institute of Technology, Newark, New Jersey 07102-1982, United States;* orcid.org/0000-0002-8765-3922; Email: cld@njit.edu

Authors

Sharareh Jalali − *Department of Physics, New Jersey Institute of Technology, Newark, New Jersey 07102-1982, United States;* orcid.org/0000-0001-7185-0692

Ruoyao Zhang − *Department of Mechanical and Aerospace Engineering, Princeton University, Princeton, New Jersey 08544, United States*

Mikko P. Haataja − *Department of Mechanical and Aerospace Engineering and Princeton Materials Institute, Princeton University, Princeton, New Jersey 08544, United States;* orcid.org/0000-0001-8459-7331

Complete contact information is available at: https://pubs.acs.org/10.1021/acs.jpcb.3c05300

Notes

The authors declare no competing financial interest.

■ ACKNOWLEDGMENTS

S.J. and C.D. were supported by the National Institute of General Medical Health under grant no. 1R15GM148982-01. Computational resources were provided by the Academic and Research Computing System (ARCS) at the New Jersey Institute of Technology and by the Pittsburgh Supercomputing Center (PSC). Anton 2 at PSC is supported by the National Institute of General Medical Sciences of the National Institute of Health under Award number R01GM116961. The Anton 2 machine at PSC was generously made available by D.E. Shaw Research. R.Z. and M.P.H. were primarily supported by NSF through the Princeton University (PCCM) Materials Research Science and Engineering Center DMR-2011750.

■ REFERENCES

(1) Ilie, I. M.; Caflisch, A. Simulation Studies of Amyloidogenic Polypeptides and Their Aggregates. *Chem. Rev.* **2019**, *119*, 6956−6993.

(2) Nguyen, P. H.; Ramamoorthy, A.; Sahoo, B. R.; Zheng, J.; Faller, P.; Straub, J. E.; Dominguez, L.; Shea, J.-E.; Dokholyan, N. V.; De Simone, A.; et al. Amyloid Oligomers: A Joint Experimental/Computational Perspective on Alzheimer's Disease, Parkinson's Disease, Type II Diabetes, and Amyotrophic Lateral Sclerosis. *Chem. Rev.* **2021**, *121*, 2545−2647.

(3) Owen, M. C.; Gnutt, D.; Gao, M.; Wärmländer, S. K. T. S.; Jarvet, J.; Gräslund, A.; Winter, R.; Ebbinghaus, S.; Strodel, B. Effects of in Vivo Conditions on Amyloid Aggregation. *Chem. Soc. Rev.* **2019**, *48*, 3946−3996.

(4) Cao, Y.; Tang, X.; Yuan, M.; Han, W. Computational studies of protein aggregation mediated by amyloid: fibril elongation and secondary nucleation. *Prog. Mol. Biol. Transl. Sci.* **2020**, *170*, 461−504.

(5) Morriss-Andrews, A.; Shea, J.-E. Simulations of Protein Aggregation: Insights from Atomistic and Coarse-Grained Models. *J. Phys. Chem. Lett.* **2014**, *5*, 1899−1908.

(6) Zottig, X.; Côté-Cyr, M.; Arpin, D.; Archambault, D.; Bourgault, S. Protein Supramolecular Structures: From Self-Assembly to Nanovaccine Design. *Nanomaterials* **2020**, *10*, 1008.

(7) Kushner, A. M.; Guan, Z. Modular design in natural and biomimetic soft materials. *Angew. Chem., Int. Ed.* **2011**, *50*, 9026−9057.

(8) Edwards-Gayle, C. J.; Hamley, I. W. Self-assembly of bioactive peptides, peptide conjugates, and peptide mimetic materials. *Org. Biomol. Chem.* **2017**, *15*, 5867−5876.

(9) Dehsorkhi, A.; Castelletto, V.; Hamley, I. W. Self-assembling amphiphilic peptides. *J. Pept. Sci.* **2014**, *20*, 453−467.

(10) Marshall, K. E.; Vadukul, D. M.; Dahal, L.; Theisen, A.; Fowler, M. W.; Al-Hilaly, Y.; Ford, L.; Kemenes, G.; Day, I. J.; Staras, K.; et al. A critical role for the self-assembly of Amyloid-β1−42 in neurodegeneration. *Sci. Rep.* **2016**, *6* (1), 30182.

(11) Deng, L.; Zhou, P.; Zhao, Y.; Wang, Y.; Xu, H. Molecular origin of the self-assembled morphological difference caused by varying the order of charged residues in short peptides. *J. Phys. Chem. B* **2014**, *118*, 12501−12510.

(12) Whitesides, G. M.; Boncheva, M. Beyond molecules: Self-assembly of mesoscopic and macroscopic components. *Proc. Natl. Acad. Sci. U.S.A.* **2002**, *99*, 4769−4774.

(13) Zhang, S.; Marini, D. M.; Hwang, W.; Santoso, S. Design of nanostructured biological materials through self-assembly of peptides and proteins. *Curr. Opin. Chem. Biol.* **2002**, *6* (6), 865−871.

(14) Törnquist, M.; Michaels, T. C. T.; Sanagavarapu, K.; Yang, X.; Meisl, G.; Cohen, S. I. A.; Knowles, T. P. J.; Linse, S. Secondary Nucleation in Amyloid Formation. *Chem. Commun.* **2018**, *54*, 8667−8684.

(15) Michaels, T. C. T.; Šarić, A.; Curk, S.; Bernfur, K.; Arosio, P.; Meisl, G.; Dear, A. J.; Cohen, S. I. A.; Dobson, C. M.; Vendruscolo, M.; et al. Dynamics of Oligomer Populations Formed during the Aggregation of Alzheimer's Aβ42 Peptide. *Nat. Chem.* **2020**, *12*, 445−451.

(16) Linse, S.; Scheidt, T.; Bernfur, K.; Vendruscolo, M.; Dobson, C. M.; Cohen, S. I.; Sileikis, E.; Lundqvist, M.; Qian, F.; O'Malley, T.; et al. Kinetic Fingerprints Differentiate the Mechanisms of Action of Anti-Aβ Antibodies. *Nat. Struct. Mol. Biol.* **2020**, *27*, 1125−1133.

(17) Sulatsky, M. I.; Stepanenko, O. V.; Stepanenko, O. V.; Mikhailova, E. V.; Kuznetsova, I. M.; Turoverov, K. K.; Sulatskaya, A. I. Amyloid fibrils degradation: the pathway to recovery or aggravation of the disease? *Front. Mol. Biosci.* **2023**, *10*, 1208059.

(18) Strodel, B. Amyloid Aggregation Simulations: Challenges, Advances and Perspectives. *Curr. Opin. Struct. Biol.* **2021**, *67*, 145−152.

(19) Williams-Noonan, B. J.; Kamboukos, A.; Todorova, N.; Yarovsky, I. Self-Assembling Peptide Biomaterials: Insights from Spontaneous and Enhanced Sampling Molecular Dynamics Simulations. *Chem. Phys. Rev.* **2023**, *4*, 021304.

(20) Jalali, S.; Yang, Y.; Mahmoudinobar, F.; Singh, S. M.; Nilsson, B. L.; Dias, C. Using All-Atom Simulations in Explicit Solvent to Study Aggregation of Amphipathic Peptides into Amyloid-like Fibrils. *J. Mol. Liq.* **2022**, *347*, 118283.

(21) Carballo-Pacheco, M.; Strodel, B. Advances in the Simulation of Protein Aggregation at the Atomistic Scale. *J. Phys. Chem. B* **2016**, *120*, 2991−2999.

(22) Samantray, S.; Yin, F.; Kav, B.; Strodel, B. Different Force Fields Give Rise to Different Amyloid Aggregation Pathways in Molecular Dynamics Simulations. *J. Chem. Inf. Model.* **2020**, *60*, 6462−6475.
(23) Pellarin, R.; Guarnera, E.; Caflisch, A. Pathways and Intermediates of Amyloid Fibril Formation. *J. Mol. Biol.* **2007**, *374*, 917−924.
(24) Pellarin, R.; Caflisch, A. Interpreting the Aggregation Kinetics of Amyloid Peptides. *J. Mol. Biol.* **2006**, *360*, 882−892.
(25) Han, W.; Schulten, K. Fibril Elongation by Aβ17−42: Kinetic Network Analysis of Hybrid-Resolution Molecular Dynamics Simulations. *J. Am. Chem. Soc.* **2014**, *136*, 12450−12460.
(26) Urbic, T.; Najem, S.; Dias, C. L. Thermodynamic Properties of Amyloid Fibrils in Equilibrium. *Biophys. Chem.* **2017**, *231*, 155−160.
(27) Šarić, A.; Michaels, T. C. T.; Zaccone, A.; Knowles, T. P. J.; Frenkel, D. Kinetics of Spontaneous Filament Nucleation via Oligomers: Insights from Theory and Simulation. *J. Chem. Phys.* **2016**, *145*, 211926.
(28) Nguyen, P.; Derreumaux, P. Understanding amyloid fibril nucleation and Aβ oligomer/drug interactions from computer simulations. *Acc. Chem. Res.* **2014**, *47*, 603−611.
(29) Wang, Y.; Bunce, S. J.; Radford, S. E.; Wilson, A. J.; Auer, S.; Hall, C. K. Thermodynamic Phase Diagram of Amyloid-β (16−22) Peptide. *Proc. Natl. Acad. Sci. U.S.A.* **2019**, *116*, 2091−2096.
(30) Bunce, S. J.; Wang, Y.; Stewart, K. L.; Ashcroft, A. E.; Radford, S. E.; Hall, C. K.; Wilson, A. J. Molecular Insights into the Surface-Catalyzed Secondary Nucleation of Amyloid-β40 (Aβ40) by the Peptide Fragment Aβ16−22. *Sci. Adv.* **2019**, *5*, No. eaav8216.
(31) Mahmoudinobar, F.; Urban, J. M.; Su, Z.; Nilsson, B. L.; Dias, C. L. Thermodynamic Stability of Polar and Nonpolar Amyloid Fibrils. *J. Chem. Theory Comput.* **2019**, *15*, 3868−3874.
(32) Su, Z.; Dias, C. L. Driving β-Strands into Fibrils. *J. Phys. Chem. B* **2014**, *118*, 10830−10836.
(33) Narayanan, C.; Dias, C. L. Hydrophobic Interactions and Hydrogen Bonds in β-Sheet Formation. *J. Chem. Phys.* **2013**, *139*, 115103.
(34) Schwierz, N.; Frost, C. V.; Geissler, P. L.; Zacharias, M. Dynamics of Seeded Aβ40-Fibril Growth from Atomistic Molecular Dynamics Simulations: Kinetic Trapping and Reduced Water Mobility in the Locking Step. *J. Am. Chem. Soc.* **2016**, *138*, 527−539.
(35) Schwierz, N.; Frost, C. V.; Geissler, P. L.; Zacharias, M. From Aβ Filament to Fibril: Molecular Mechanism of Surface-Activated Secondary Nucleation from All-Atom MD Simulations. *J. Phys. Chem. B* **2017**, *121*, 671−682.
(36) Lemkul, J. A.; Bevan, D. R. Assessing the Stability of Alzheimer's Amyloid Protofibrils Using Molecular Dynamics. *J. Phys. Chem. B* **2010**, *114*, 1652−1660.
(37) Tang, X.; Han, W. Multiscale Exploration of Concentration-Dependent Amyloid-β(16−21) Amyloid Nucleation. *J. Phys. Chem. Lett.* **2022**, *13*, 5009−5016.
(38) Barz, B.; Liao, Q.; Strodel, B. Pathways of Amyloid-β Aggregation Depend on Oligomer Shape. *J. Am. Chem. Soc.* **2018**, *140*, 319−327.
(39) Bernstein, S. L.; Dupuis, N. F.; Lazo, N. D.; Wyttenbach, T.; Condron, M. M.; Bitan, G.; Teplow, D. B.; Shea, J.-E.; Ruotolo, B. T.; Robinson, C. V.; et al. Amyloid-β Protein Oligomerization and the Importance of Tetramers and Dodecamers in the Aetiology of Alzheimer's Disease. *Nat. Chem.* **2009**, *1*, 326−331.
(40) Sun, Y.; Kakinen, A.; Xing, Y.; Pilkington, E. H.; Davis, T. P.; Ke, P. C.; Ding, F. Nucleation of β-rich oligomers and β-barrels in the early aggregation of human islet amyloid polypeptide. *Biochim. Biophys. Acta, Mol. Basis Dis.* **2019**, *1865*, 434−444.
(41) Wei, G.; Mousseau, N.; Derreumaux, P. Sampling the self-assembly pathways of KFFE hexamers. *Biophys. J.* **2004**, *87*, 3648−3656.
(42) Cohen, S. I. A.; Linse, S.; Luheshi, L. M.; Hellstrand, E.; White, D. A.; Rajah, L.; Otzen, D. E.; Vendruscolo, M.; Dobson, C. M.; Knowles, T. P. J. Proliferation of Amyloid-β42 Aggregates Occurs through a Secondary Nucleation Mechanism. *Proc. Natl. Acad. Sci. U.S.A.* **2013**, *110*, 9758−9763.
(43) Yamazaki, M.; Ikeda, K.; Kameda, T.; Nakao, H.; Nakano, M. Kinetic Mechanism of Amyloid-β-(16−22) Peptide Fibrillation. *J. Phys. Chem. Lett.* **2022**, *13*, 6031−6036.
(44) Wetzel, R. Kinetics and Thermodynamics of Amyloid Fibril Assembly. *Acc. Chem. Res.* **2006**, *39*, 671−679.
(45) Young, L. J.; Kaminski Schierle, G. S.; Kaminski, C. F. Imaging Aβ (1−42) Fibril Elongation Reveals Strongly Polarised Growth and Growth Incompetent States. *Phys. Chem. Chem. Phys.* **2017**, *19*, 27987−27996.
(46) Buell, A. K.; Galvagnion, C.; Gaspar, R.; Sparr, E.; Vendruscolo, M.; Knowles, T. P.; Linse, S.; Dobson, C. M. Solution conditions determine the relative importance of nucleation and growth processes in α-synuclein aggregation. *Proc. Natl. Acad. Sci. U.S.A.* **2014**, *111*, 7671−7676.
(47) Qiang, W.; Kelley, K.; Tycko, R. Polymorph-specific kinetics and thermodynamics of β-amyloid fibril growth. *J. Am. Chem. Soc.* **2013**, *135*, 6860−6871.
(48) Esler, W. P.; Stimson, E. R.; Jennings, J. M.; Vinters, H. V.; Ghilardi, J. R.; Lee, J. P.; Mantyh, P. W.; Maggio, J. E. Alzheimer's disease amyloid propagation by a template-dependent dock-lock mechanism. *Biochemistry* **2000**, *39*, 6288−6295.
(49) Schmit, J. D. Kinetic Theory of Amyloid Fibril Templating. *J. Chem. Phys.* **2013**, *138*, 185102.
(50) Jia, Z.; Schmit, J. D.; Chen, J. Amyloid Assembly Is Dominated by Misregistered Kinetic Traps on an Unbiased Energy Landscape. *Proc. Natl. Acad. Sci. U.S.A.* **2020**, *117*, 10322−10328.
(51) Massi, F.; Straub, J. E. Energy landscape theory for Alzheimer's amyloid β-peptide fibril elongation. *Proteins: Struct., Funct., Bioinf.* **2001**, *42*, 217−229.
(52) Straub, J. E.; Thirumalai, D. Toward a molecular theory of early and late events in monomer to amyloid fibril formation. *Annu. Rev. Phys. Chem.* **2011**, *62*, 437−463.
(53) Barz, B.; Strodel, B. Understanding Amyloid-β Oligomerization at the Molecular Level: The Role of the Fibril Surface. *Chem.—Eur. J.* **2016**, *22*, 8768−8772.
(54) Jalali, S.; Yang, Y.; Mahmoudinobar, F.; Singh, S. M.; Nilsson, B. L.; Dias, C. Using all-atom simulations in explicit solvent to study aggregation of amphipathic peptides into amyloid-like fibrils. *J. Mol. Liq.* **2022**, *347*, 118283.
(55) Marini, D. M.; Hwang, W.; Lauffenburger, D. A.; Zhang, S.; Kamm, R. D. Left-Handed Helical Ribbon Intermediates in the Self-Assembly of a β-Sheet Peptide. *Nano Lett.* **2002**, *2*, 295−299.
(56) Zhang, S.; Marini, D. M.; Hwang, W.; Santoso, S. Design of Nanostructured Biological Materials through Self-Assembly of Peptides and Proteins. *Curr. Opin. Chem. Biol.* **2002**, *6* (6), 865−871.
(57) Bowerman, C. J.; Ryan, D. M.; Nissan, D. A.; Nilsson, B. L. The Effect of Increasing Hydrophobicity on the Self-Assembly of Amphipathic β-Sheet Peptides. *Mol. BioSyst.* **2009**, *5*, 1058−1069.
(58) Bowerman, C. J.; Liyanage, W.; Federation, A. J.; Nilsson, B. L. Tuning β-Sheet Peptide Self-Assembly and Hydrogelation Behavior by Modification of Sequence Hydrophobicity and Aromaticity. *Biomacromolecules* **2011**, *12*, 2735−2745.
(59) Wang, F.; Gnewou, O.; Wang, S.; Osinski, T.; Zuo, X.; Egelman, E. H.; Conticello, V. P. Deterministic Chaos in the Self-Assembly of β Sheet Nanotubes from an Amphipathic Oligopeptide. *Matter* **2021**, *4*, 3217−3231.
(60) Lindorff-Larsen, K.; Piana, S.; Palmo, K.; Maragakis, P.; Klepeis, J. L.; Dror, R. O.; Shaw, D. E. Improved side-chain torsion potentials for the Amber ff99SB protein force field. *Proteins: Struct., Funct., Bioinf.* **2010**, *78*, 1950−1958.
(61) Parrinello, M.; Rahman, A. Polymorphic transitions in single crystals: A new molecular dynamics method. *J. Appl. Phys.* **1981**, *52*, 7182−7190.
(62) Allen, M. P.; Tildesley, D. J. *Computer Simulation of Liquids*; Oxford University Press: Oxford, United Kingdom, 2017.
(63) Bjelkmar, P.; Larsson, P.; Cuendet, M. A.; Hess, B.; Lindahl, E. Implementation of the CHARMM force field in GROMACS: analysis

https://doi.org/10.1021/acs.jpcb.3c05300
J. Phys. Chem. B XXXX, XXX, XXX−XXX

of protein stability effects from correction maps, virtual interaction sites, and water models. *J. Chem. Theory Comput.* **2010**, *6*, 459−466.
(64) Abraham, M. J.; Murtola, T.; Schulz, R.; Páll, S.; Smith, J. C.; Hess, B.; Lindahl, E. GROMACS: High Performance Molecular Simulations through Multi-Level Parallelism from Laptops to Supercomputers. *SoftwareX* **2015**, *1−2*, 19−25.
(65) Eisenberg, D. S.; Sawaya, M. R. Structural studies of amyloid proteins at the molecular level. *Annu. Rev. Biochem.* **2017**, *86*, 69−95.
(66) Sengupta, U.; Carballo-Pacheco, M.; Strodel, B. Automated Markov state models for molecular dynamics simulations of aggregation and self-assembly. *J. Chem. Phys.* **2019**, *150*, 115101.
(67) Dill, K. A. Dominant Forces in Protein Folding. *Biochemistry* **1990**, *29*, 7133−7155.
(68) Kauzmann, W. *Advances in Protein Chemistry*; Academic Press, 1959.
(69) Dias, C. L.; Ala-Nissila, T.; Wong-ekkabut, J.; Vattulainen, I.; Grant, M.; Karttunen, M. The Hydrophobic Effect and Its Role in Cold Denaturation. *Cryobiology* **2010**, *60*, 91−99.
(70) Dias, C. L.; Hynninen, T.; Ala-Nissila, T.; Foster, A. S.; Karttunen, M. Hydrophobicity within the Three-Dimensional Mercedes-Benz Model: Potential of Mean Force. *J. Chem. Phys.* **2011**, *134*, 065106.
(71) Dias, C. L.; Ala-Nissila, T.; Karttunen, M.; Vattulainen, I.; Grant, M. Microscopic Mechanism for Cold Denaturation. *Phys. Rev. Lett.* **2008**, *100*, 118101.
(72) R Zhang, C. D., S Jalali; Haataja, M. Growth kinetics of amyloid-like fibrils: An integrated atomistic simulation and continuum theory approach. Submitted **2023**.

https://doi.org/10.1021/acs.jpcb.3c05300
J. Phys. Chem. B XXXX, XXX, XXX−XXX